ACS Photonics

pubs.acs.org/journal/apchd5

Letter

Low-Cost RoHS Compliant Solution Processed Photovoltaics Enabled by Ambient Condition Synthesis of $AgBiS_2$ Nanocrystals

M. Zafer Akgul, Alberto Figueroba, Santanu Pradhan, Yu Bi, and Gerasimos Konstantatos*

Cite This: *ACS Photonics* 2020, 7, 588–595

Read Online

ACCESS | Metrics & More | Article Recommendations | Supporting Information

ABSTRACT: Two major challenges exist before colloidal nanocrystal solar cells can take their place in the market: So far, these devices are based on Pb/Cd-containing nanocrystals, and second, the synthesis of these nanocrystals takes place in an inert atmosphere at elevated temperatures due to the use of air-sensitive chemicals. In this report, a room-temperature, ambient-air synthesis for nontoxic $AgBiS_2$ nanocrystals is presented. As this method utilizes stable precursors, the need for the use of a protective environment is eliminated, enabling the large-scale production of $AgBiS_2$ nanocrystals. The production cost of $AgBiS_2$ NCs at room temperature and under ambient conditions reduces by ∼60% compared to prior reports based on hot injection, and the solar cells made of these nanocrystals yield a promising power conversion efficiency (PCE) of 5.5%, the highest reported to date for a colloidal nanocrystal material free of Pb or Cd synthesized at room temperature and under ambient conditions.

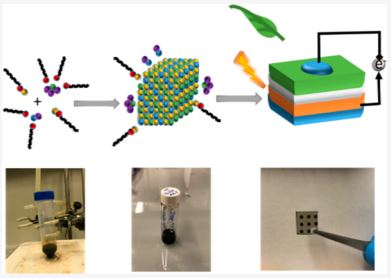

KEYWORDS: *nontoxic, room temperature, semiconductors, nanocrystals, solar cells*

Inorganic solution processed solar cells hold great promise toward high-performance, low-cost photovoltaics technologies. Colloidal Quantum Dot (CQD) solar cells are one representative technology of this class of solar cells, with reports from lead sulfide (PbS) solar cells exceeding 10% PCE.[1,2] At the same time, the development of solution-processed Pb-perovskites has boosted the attainable PCE to more than 20% for thin film solar cells,[3−5] demonstrating the potential of solution-processed materials for the solar-to-electrical energy conversion. However, environmental regulatory concerns have been raised due to the presence of toxic heavy metals in such technologies, opening an opportunity for exploration of restriction of hazardous substances (RoHS) compliant environmentally friendly alternatives. For this purpose, ternary $I-III-VI_2$ and quaternary $I_2-II-IV-VI_4$ metal chalcogenide compounds have been put under investigation, as they are less toxic than their Pb counterparts. Among nanocrystal-based technologies, copper indium disulfide (CIS), copper zinc tin sulfide (CZTS), and derivatives have driven the solution-processed photovoltaics research thanks to their attractive optical properties.[6−12] However, the realization of an efficient all solid-state nanocrystal solar cell that does not require an inert fabrication environment and high-temperature sintering has remained a challenge.[13,14]

As an alternative with similar properties to aforementioned materials, $AgBiS_2$ has been suggested as a promising nontoxic material for solution-processed solar cells. Early reports based on the Successive Ionic Layer Adsorption and Reaction (SILAR) method[15] and spray deposition[16] of $AgBiS_2$ employed as a light harvesting layer could yield a maximum PCE of 1.7%. With the utilization of hot injection method for the synthesis, PCE of $AgBiS_2$ nanocrystal solar cells has been boosted to 6.3%, proving to be a promising contender for nontoxic solution processed solar cells.[17] However, the requirement for costly chemical precursors (such as HMS, hexamethyldisilathiane) along with the use of high-temperature, vacuum, and noble gases still remains as an effort-demanding problem to be solved for the commercial viability of this technology, as a recent study has pinpointed the synthesis-related cost as a major bottleneck for the successful commercialization of solar cells based on colloidal quantum dots/nanocrystals.[18] Although it is not easy to circumvent the requisite of protective reaction environment for nanocrystals due to oxidation and degradation, $AgBiS_2$ offers an opportunity thanks to its inertness under ambient conditions.[19] By taking advantage of the inertness of $AgBiS_2$, previous attempts have shown an ambient synthesis of $AgBiS_2$ nanocrystals. Lei et al. demonstrated the possibility of synthesizing very small $AgBiS_2$ colloids at room temperature using polyethylenimine (PEI) as the ligand for in vivo imaging and photothermal therapy.[20] Later, Mak et al. published a study on graphene transistors sensitized with $AgBiS_2$ nanocrystals synthesized under ambient conditions, although the preparation of the precursor solution required a temperature of 120 °C.[21] Yet, the production of solar cell-grade $AgBiS_2$ nanocrystals performed entirely at room temperature and under ambient conditions has remained

Received: December 12, 2019
Published: March 4, 2020

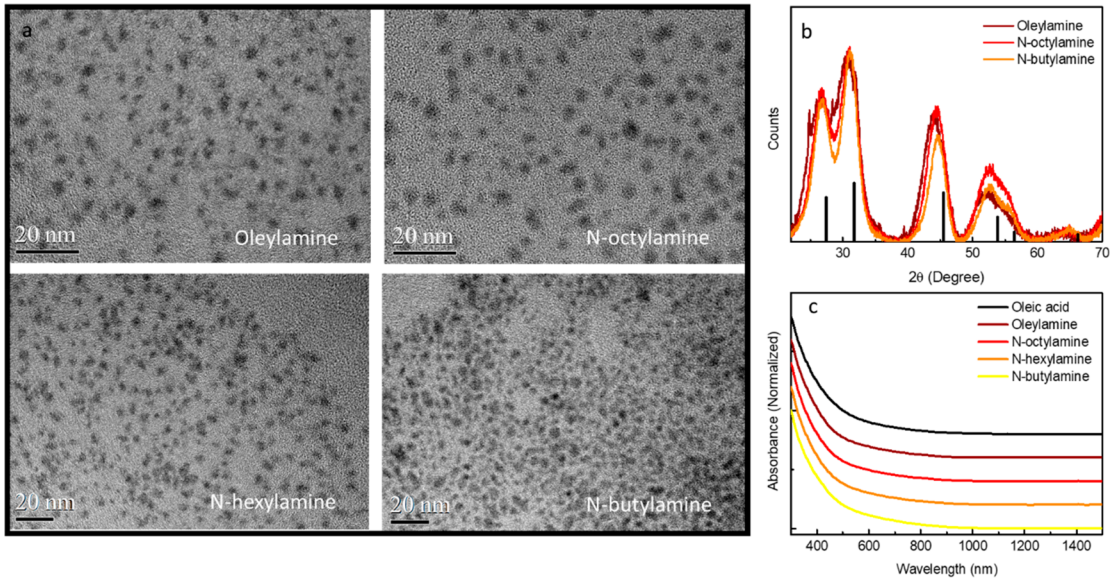

Figure 1. Structural and optical characterization of room-temperature $AgBiS_2$ nanocrystals. (a) TEM images showing the near-spherical shapes of nanocrystals synthesized using different amines (upper left, oleylamine; upper right, *n*-octylamine; lower left, *n*-hexylamine; lower right, *n*-butylamine); (b) XRD spectra of $AgBiS_2$ nanocrystals synthesized via our new room-temperature technique using different amines (brown, oleylamine; red, *n*-octylamine; orange, *n*-butylamine; black bars show the peak positions of the bulk $AgBiS_2$); and (c) Comparison of the absorbance spectra of $AgBiS_2$ nanocrystals in octane, which are synthesized via different methods (black, via Schlenk-line; brown, red, orange, and yellow, room-temperature method using oleylamine, *n*-octylamine, *n*-hexylamine, and *n*-butylamine, respectively; curves are plotted with offset for ease of viewing).

elusive. In this work, we concomitantly address the aforementioned challenges by developing a solution processed solar cell that is based on environmentally friendly $AgBiS_2$ nanocrystals that are produced via low-cost, readily up-scalable synthetic chemistry under ambient and room temperature conditions using only commercially available precursors.

As the previously reported hot-injection synthesis requires a high reaction temperature and an air-sensitive sulfur precursor to achieve photovoltaic-quality nanocrystals the use of a protective environment is mandatory. To overcome the limitation for an inert reaction environment, we sought to use air-stable precursors that can be activated at room temperature. To perform a successful reaction at room temperature without the need of a protective environment, HMS must be replaced with an air-stable sulfur precursor. A very common strategy utilized in the literature is to use a solution of elemental sulfur in amines, as it is advantageous to utilize cheap, abundant, and nontoxic materials as the precursors.[22−24] In this scheme, amines can act as soft ligands during the synthesis to prevent nuclei from coalescing; hence, no other chemicals are needed for the growth of the nanocrystals. To probe the effect of the ligand, we synthesized $AgBiS_2$ nanocrystals using amines with different chain lengths, as the ligands used during the nucleation and growth of nanocrystals can have an effect on the nanocrystal size. Thanks to the solubility of the silver and bismuth iodides in amines, we could successfully cover a wide range of amines with varying chain length, starting from 4-carbon butylamine up to 18-carbon oleylamine. (However, the nanocrystal dispersions tend to aggregate after purification steps, as the amines are loosely attached to the nanocrystal surface. To improve the colloidal stability for further characterization and processing, an in situ ligand exchange with 1-octanethiol is performed just before purification.) For all amines, near-spherical $AgBiS_2$ nanocrystals were obtained (Figure 1a). Transmission electron microscopy (TEM) images indicated that the size of the nanocrystals can be increased by employing shorter chain amines, as expected, thanks to the less steric hindrance effect of a shorter carbon backbone.[25] The crystal size of the respective $AgBiS_2$ dispersions was also confirmed via X-ray Diffraction (XRD) measurements using Sherrer equation.

$$d = \frac{K\lambda}{\beta \cos(\theta)}$$

Here, d is the crystal size, K is a dimensionless shape factor (0.9), λ is the wavelength of the X-ray source (0.15046 nm), β is the full-width at half-maximum in radians, and θ is the Bragg angle. The tuning range of the nanocrystal size was found to be 2.5−3.2 nm for oleylamine and *n*-butylamine, respectively (Table 1 and Figure 1b). As it can be seen from Figure 1c, the absorption characteristics of the $AgBiS_2$ nanocrystals measured in solution are very similar for hot-injection and room-temperature syntheses. A bandgap of 1.2 eV is obtained from the Tauc plot for room-temperature nanocrystals, which is suitable for single-junction photovoltaics (Figure S1). Thanks to its commercial availability, low cost, low evaporation, and

Table 1. Size Comparison of $AgBiS_2$ Nanocrystals Synthesized via Schlenk-Line and Room-Temperature Methods Using Different Amines[a]

sample	nanocrystal size (XRD; nm)	nanocrystal size (TEM; nm)	std dev (TEM; nm)
oleic acid	4.34	4.60	0.94
n-butylamine	3.11	3.26	0.93
n-octylamine	2.53	2.96	0.90
oleylamine	2.55	2.54	0.82

[a]The nanocrystal size decreases with the increasing chain length of the amine.

https://dx.doi.org/10.1021/acsphotonics.9b01757
ACS Photonics 2020, 7, 588−595

suitable viscosity at room temperature, we found that *n*-octylamine is the best among the amines utilized in this study for the synthesis of $AgBiS_2$ nanocrystals. For this reason, we optimized the rest of our processes for the nanocrystals synthesized using *n*-octylamine.

X-ray Photoelectron Spectroscopy (XPS) analysis shows that $AgBiS_2$ nanocrystals synthesized at room temperature are bismuth-rich (1:1.30), unlike Ag-rich nanocrystals obtained via a hot-injection method (1:0.78; Table 2). Ag-3d gives a single doublet (at 368.0 eV, Figure 2a,b) for both types of nanocrystals. Two doublets are required to fit the bismuth-4f peaks (at ∼158.0 and ∼159.0 eV, the ratios of the areas of the doublets are 0.53 for room-temperature and 0.46 for Schlenk-line nanocrystals, Figure 2c,d). The main component of the S-2s signal of room-temperature nanocrystals shows a small shift from that of Schlenk-line nanocrystals (225.3 and 225.4 eV; see Figure 2e,f). Moreover, the sulfur content of the room-temperature nanocrystals was found to be higher than that of Schlenk-line nanocrystals (1.49 vs 1.05), which may result from the presence of thiols on the surface.

Table 2. XPS Analysis (Normalized to Ag 3d Peaks) of $AgBiS_2$ Nanocrystals Synthesized via Schlenk-Line (Oleic Acid, Treated with TMAI) and Room-Temperature (*n*-Octylamine, Treated with Ethanethiol) Methods[a]

sample	Ag (3d)	Bi (4f)	S (2p)
oleic acid	1.00	0.78	1.05
n-octylamine	1.00	1.30	1.49

[a]The results show that the Schlenk-line method gives Ag-rich nanocrystals, whereas the room-temperature method yields Bi-rich nanocrystals.

The activation of elemental sulfur by amines is a key step in the synthesis of metal sulfide nanocrystals at room temperature. According to a study published in the literature, elemental sulfur forms alkylammonium polysulfides when dissolved in amines at low temperatures.[26] Although elemental sulfur is not reactive toward silver and bismuth iodides at room temperature, alkylammonium polysulfides can react with these metal iodides under ambient conditions. As the solubility of Ag-S and Bi-S monomers is negligible in amines, the nucleation of $AgBiS_2$ occurs, which is manifested by gradual darkening of the reaction mixture. After reaction, in situ formed iodine/iodide is dissolved by the amines, possibly iodine forming a charge transfer (CT) complex with amines as described in a previous study.[27] Our findings support that alkyl ammonium iodide salts are formed as the byproduct of this reaction (Figure S2).

Although long ligands are effective in forming colloidally stable nanocrystal dispersions, it is required to have shorter ligands on the surface of the nanocrystals to facilitate the charge transfer in a photovoltaic device. In the study reported previously,[15] a tetramethylammonium iodide (TMAI) treatment was utilized to exchange long oleate groups with iodide ions. However, formation of thin films with TMAI treatment alone is not possible in our case due to the high chemical affinity of 1-octanethiol toward silver and bismuth cations compared to the iodide anions (see the experimental details for further information about synthesis). To overcome this issue, we developed a new ligand exchange method based on ethanethiol (ET) for the removal of long and insulating 1-octanethiol from the nanocrystal surface. The exchange of 1-octanethiol with ET is possible, as thiols with a shorter carbon backbone have higher affinity toward Ag and Bi. To observe the removal of 1-octanethiol from the film, a Fourier-Transform Infrared Spectroscopy (FTIR) study was carried out. To ensure that the spectrum does not have a contribution from the unbound ligands, the film was rinsed with methanol before treating with ET. No significant change was observed in the C−H peaks (within 2850−3000 cm^{-1} range) after methanol rinsing. After treatment with ET and annealing, the intensity of the C−H peaks decreased significantly, showing removal of most of the 1-octanethiol from the surface of the nanocrystals (Figure 3a). To check the quality of the film, we also prepared samples using ITO glass as the substrate. A Scanning Electron Microscope (SEM) examination demon-

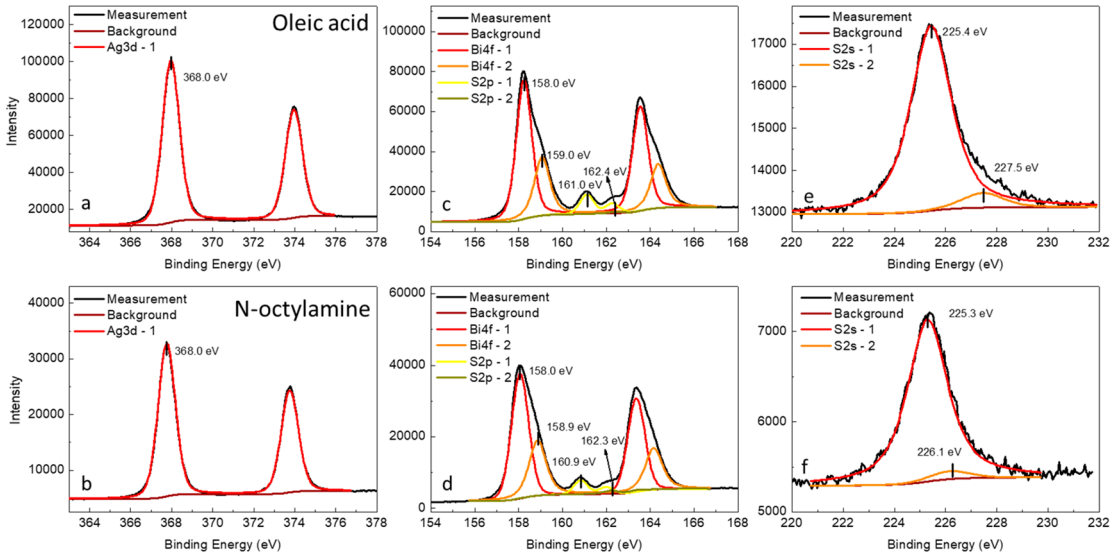

Figure 2. XPS scans of $AgBiS_2$ nanocrystals synthesized via Schlenk-line (a, silver-3d; c, bismuth-4f; e, sulfur-2s) and room-temperature (b, silver-3d; d, bismuth-4f; f, sulfur-2s) methods. All the major peaks were found to have very similar binding energies for room-temperature and Schlenk-line $AgBiS_2$ nanocrystals.

https://dx.doi.org/10.1021/acsphotonics.9b01757
ACS Photonics 2020, 7, 588−595

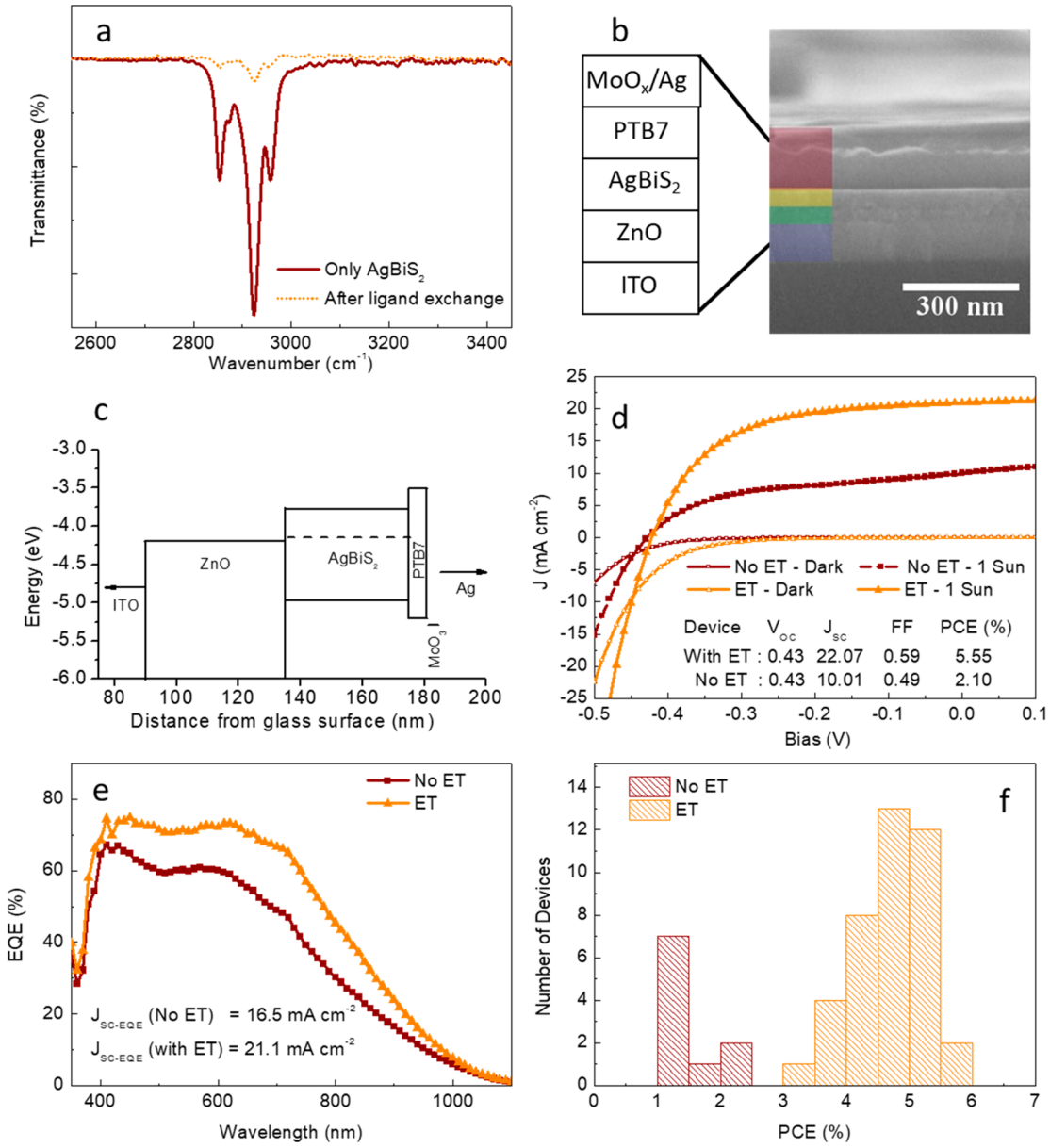

Figure 3. Characterization of the solar cell. (a) FTIR results showing the removal of most of the organics from the film (orange line, before ET; brown dotted line, after ET treatment). (b) Cross-sectional SEM image of the solar cell showing individual layers. (c) Band positions of room-temperature $AgBiS_2$ nanocrystals within the solar cell. (d) $J-V$ and (e) EQE curves and (f) device performance statistics of the room-temperature $AgBiS_2$ nanocrystal solar cells with ET (orange triangles) and without ET (brown squares) treatment 1 day after device fabrication.

strated that ET-treatment gives smooth and dense nanocrystal thin films (Figure S3).

To test the photovoltaic performance of the nanocrystals, we fabricated solar cells employing the previously reported structure, as the band levels of our room-temperature $AgBiS_2$ nanocrystals are close to those of Schlenk-line $AgBiS_2$ nanocrystals (Figure 3b,c, see Figure S4 for Ultraviolet Photoelectron Spectroscopy (UPS) measurements).[17] The possibility of using ET, a much smaller ligand compared to previously reported TMAI,[17] for the ligand exchange process allowed us to use a faster single-step deposition process by using a more concentrated dispersion (~60 g L^{-1}) to achieve the optimal $AgBiS_2$ thickness of ~40 nm, as opposed to a previously reported layer-by-layer deposition process for $AgBiS_2$.[17] With this ligand exchange, our champion $AgBiS_2$ nanocrystal solar cell gave a PCE of 4.62% just after device fabrication. After storing the solar cell under ambient conditions (24 °C, 50–60% humidity) for 1 day, the efficiency of the solar cell showed ~20% increase, reaching 5.55% without a significant hysteresis (Figures 3d and S5). With a thickness of only ~40 nm, a promising open-circuit voltage (V_{OC}) of 0.43 V and a short-circuit current (J_{SC}) of 22.07 mA cm^{-2} with a fill factor (FF) of 0.59 were attained demonstrating the success of our room-temperature technique. Also, J_{SC} obtained from external quantum efficiency (EQE) spectrum is calculated to be 21.13 mA cm^{-2}, which is close to the measured short-circuit current of 22.07 mA cm^{-2} (Figure 3e). Even after storage in air under ambient conditions for 6 days, the solar cell preserved ~80% of its maximum PCE (Figure S5). The devices produced with ET treatment yield an average PCE of 4.68 ± 0.55%, while PCE of the devices without ET treatment is found to be 1.51 ± 0.40% (Figure 3f).

https://dx.doi.org/10.1021/acsphotonics.9b01757
ACS Photonics 2020, 7, 588–595

Also, $AgBiS_2$ nanocrystal dispersions in octane exhibit good stability characteristics under long-term storage in air (Figure S6). Even after 140 days of storage under ambient conditions, the nanocrystals preserved their colloidal stability, and the solar cells made of these nanocrystals with ET treatment yielded a PCE of ∼5%.

To test the effect of ET treatment, we also fabricated solar cells without ET treatment. The solar cell without ET treatment was prepared by spin-coating nanocrystal dispersion and rinsing with pure methanol using the same process parameters used to prepare the ET-treated solar cell. As it is clearly seen from Figure 3d, the solar cell without ET treatment performed much worse than the one with ET treatment. Although both devices gave very similar V_{OC}, the solar cell without ET treatment could give a J_{SC} less than half that of the device with ET treatment. Also, we found that FF of the solar cell without ET treatment was noticeably lower than that of the solar cell with ET treatment, demonstrating that the extraction efficiency of the charge carriers within the $AgBiS_2$ layer is lower if ET treatment is not performed. This is an expected result, as the long carbon backbone of 1-octanethiol can effectively hinder charge transfer within the $AgBiS_2$ layer, causing a drop in J_{SC} and FF. Furthermore, J_{SC} calculated from EQE curve for the solar cell without ET treatment was found to be much higher than the measured J_{SC} (16.5 vs 10.01 mA cm^{-2}), indicating that a light intensity-dependent processes may be another reason for low PCE (Figure 3e). To probe the effect of the intensity of light on device performance, we carried out light intensity-dependent V_{OC}/J_{SC} measurements. For the solar cell prepared without ET treatment, the light intensity-dependent V_{OC}/J_{SC} measurements showed saturation at high light bias condition, explaining the origin of lower J_{SC} for this device at 1 Sun (Figure S7). Also, the ideality factor of this device was found to be 1.52 at low-light regime, which is an indication for the trap-mediated Shockley−Read−Hall (SRH) recombination.[28] On the other hand, the light intensity dependent V_{OC} measurement for ET-treated solar cell showed no saturation and yielded an ideality factor of 1.36, showing that ET treatment was effective at reducing SRH recombination (Figure 4a). Considering that the performance of the device was improved significantly by ET treatment only, it can be asserted that some of the traps involved in carrier loss are surface-related defects. Also, light intensity-dependent J_{SC} for an ET-treated device gave a power factor of 0.9, demonstrating that the charge carrier extraction in the structure is efficient enough for the proper operation of the solar cell.[29] The light intensity dependence of the carrier lifetime showed a single-component decay with an inverse slope of −0.115 V/decade, reaching ∼2.2 μs at 1 sun (Figure 4b). The density of states (DOS) within the bandgap is measured following a method published in the literature.[30] As expected, DOS increased significantly close to the V_{OC} at 1 sun. The measured DOS in the bandgap of $AgBiS_2$ was found to be an order of magnitude higher compared to PbS nanocrystal solar cells giving hints about the possible causes of the drop in J_{SC} with increasing thickness of the nanocrystal layer.[17,30] The effective carrier density and the built-in potential are measured to be 2.2×10^{17} cm^{-3} and 0.54 V using Mott−Schottky plot (Figure 4c, see Supporting Information for the details of the calculation). Using these values, the depletion width in the device was calculated to be ∼70 nm at zero bias. Hence, it can be concluded that these solar cells operate with a depleted $AgBiS_2$ layer, which is in accord with the apparent match of the

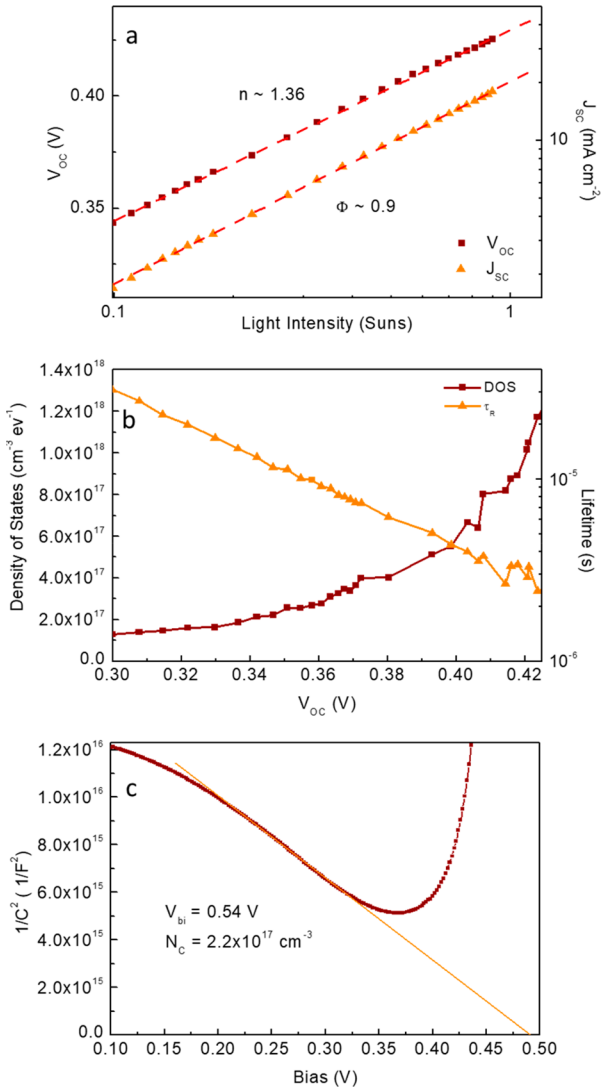

Figure 4. Electrical characteristics of the room-temperature $AgBiS_2$ nanocrystals treated with ET. (a) V_{OC} (brown squares) and J_{SC} (orange triangles) change with respect to light intensity. (b) Density of states (brown squares) within the bandgap and carrier lifetime (orange triangles) with respect to V_{OC}. (c) Mott−Schottky plot of the solar cell showing the effective carrier density (N_C) and built-in potential (V_{bi}).

measured J_{SC} and J_{SC} predicted by optical (transfer matrix method) simulations (Figure S8). Although it is sufficient to achieve a J_{SC} of 22 mA cm^{-2} and a PCE in excess of 5% with the current structure, this depletion width is not sufficient to reach a J_{SC} more than 25 mA cm^{-2}, which is predicted to be obtainable with an $AgBiS_2$ thickness of more than 150 nm. Thus, there is still some room to improve the PCE of $AgBiS_2$ NC solar cells by engineering the charge transport in the device.

Besides ease and simplicity, the synthesis cost of $AgBiS_2$ nanocrystals is also reduced by using our technique. Due to the substitution of expensive and air-sensitive HMS with cheap and abundant elemental sulfur, a cost saving of ∼98% is achieved (HMS - synthesis grade: 3322 € mol^{-1}, sulfur −99.99%: 55.4 € mol^{-1}, see Table S1 for details) for the anion precursor. Our preliminary estimations showed that a 40 nm thick $AgBiS_2$ nanocrystal film costs 11.6 € m^{-2} if the hot-injection method is utilized, whereas the costs will be reduced

https://dx.doi.org/10.1021/acsphotonics.9b01757
ACS Photonics 2020, 7, 588−595

to 4.5 € m^{-2} with a room-temperature route, showing that an overall cost saving of ∼60% can be easily achieved by substituting HMS with elemental sulfur, metal acetates with metal iodides, and oleic acid/octadecene with *n*-octylamine. Furthermore, it is expected that cost savings be even higher when the cost related to the vacuum, heating and inert reaction environment is also taken into consideration.

As a summary, we demonstrate a solution processed solar cell comprising environmentally friendly $AgBiS_2$ nanocrystals that are synthesized at room-temperature and ambient conditions. We report a new ligand exchange strategy and single-step film deposition method for our $AgBiS_2$ nanocrystals synthesized at room-temperature to remove the long ligands to form a close-packed photovoltaic quality absorber layer. The fabricated devices show a promising power conversion efficiency in excess of 5% and demonstrated that the synthesis-related cost can be reduced significantly using air-stable chemicals for the synthesis of nanocrystals. Our work paves the way toward solar cell absorbers that are at the same time cheap to produce and environmentally friendly both from a material and production perspectives and address the regulatory concerns and synthetic cost of colloidal nanocrystals based on Schlenk-line approaches.

METHODS

Chemicals and Materials. All reagents were purchased from Sigma-Aldrich, except $Bi(OAc)_3$ which was purchased from Alfa Aesar and AgI which was obtained from Strem Chemicals. PTB7 (poly[(4,8-bis(2-ethylhexyloxy)-benzo(1,2-*b*:4,5-*b*′)dithiophene)-2,6-diyl-*alt*-(4-(2-ethylhexyl)-3-fluorothieno[3,4-*b*]thiophene-)-2-carboxylate-2−6-diyl)]) was purchased from 1-material.

Synthesis of $AgBiS_2$ Nanocrystals Based on Hot Injection. For hot-injection synthesis, silver acetate (0.8 mmol), bismuth(III) acetate (1 mmol), and oleic acid (17 mmol) were charged into a three-neck flask, as described previously.[17] The flask was pumped down at 90 °C to eliminate the air and moisture from the reaction environment. After the formation of metal-oleates, the flask was filled with argon gas, and the temperature was ramped up to 100 °C. Then, a solution of HMS (1 mmol) in 1-octadecene (5 mL) was prepared in a drybox and swiftly injected into the flask. The flask was left to cool down to room temperature. $AgBiS_2$ nanocrystals were separated from the reaction mixture with addition of ethanol and centrifugation. The nanocrystals were dispersed in toluene with a concentration of 20 g L^{-1} and the dispersion was filtered through 0.2 μm PTFE filter and used as it is.

Synthesis of $AgBiS_2$ Nanocrystals Based on Room Temperature and Ambient Atmosphere. For room-temperature synthesis, AgI (0.2 mmol) and BiI_3 (0.2 mmol) were dissolved in amines (4 mL) and stirred. In a separate vial, a sulfur-amine solution (4 mol L^{-1}) was prepared. A suitable portion of this solution (80 μL) was swiftly injected into vigorously stirring AgI−BiI_3 mixture. Then, 1-octanethiol (0.15 mL) was added, and the $AgBiS_2$ nanocrystals were separated by the addition of acetonitrile and centrifugation. Nanocrystals were dispersed in octane with a concentration of 60 g L^{-1} and filtered through 0.2 μm PTFE filter.

Device Fabrication. ITO substrates were cleaned by sonication in soapy water, DI water, acetone, and isopropanol sequentially. Then, a solution of Zn^{2+} was prepared in a glovebox by dissolving $Zn(acetate)_2{\cdot}2H_2O$ (500 mg) in 2-methoxyethanol (5 mL) and ethanolamine (142 μL). This solution was spread on cleaned ITO substrates via spin coating at 3000 rpm for 30 s. After spin coating, the substrates were placed on top of a hot plate at 200 °C. After 30 min of annealing, the substrates were left to cool down and the same procedure was repeated one more time to obtain a ZnO thickness of 45 nm. TMAI-treated $AgBiS_2$ films were deposited via multiple spin coating steps following the recipe of the previously published study.[17] For the deposition of the ET-treated solar cells, we utilized a faster route. Basically, one drop of concentrated $AgBiS_2$ dispersion was dropped onto ZnO-coated substrate spinning at 2000 rpm. Then, the spinning was stopped and ethanethiol (ET; 0.2% in methanol, 5 drops) was dispensed. After 15 s of soaking, the sample was spun to dryness. Then, the sample was rinsed with methanol and spun to dryness. After the deposition, $AgBiS_2$ film was annealed on a hot plate in air at 100 °C for 10 min. Then, a hole transport layer was deposited by spin coating a PTB7 solution (5 g L^{-1} in dichlorobenzene) at 2000 rpm. Top contact was formed by thermally evaporating MoO_3 (3 nm) and Ag (150 nm) using a Kurt J. Lesker Nano36 thermal evaporator. A shadow mask with 2 mm circular holes was used to define the top contact profile.

Material Characterization. UV−vis absorption spectrum was measured using a Cary 5000 spectrophotometer using 1 cm optical path cuvettes using dilute nanocrystal dispersions in octane. TEM was performed using a JEOL 2100 microscope with an acceleration voltage of 200 kV at the Scientific and Technological Center of the University of Barcelona (CCiT-UB). Samples were prepared by dropcasting dilute $AgBiS_2$ dispersions onto carbon-coated copper grids. XRD spectra were obtained using a PANalytical X'Pert PRO MPD Alpha1 powder diffractometer with Cu Kα radiation (λ = 1.5406 Å, 45 kV, 40 mA). The samples were prepared by dropcasting a concentrated dispersion of $AgBiS_2$ nanocrystals onto glass slides. X-ray and Ultraviolet photoelectron spectroscopy (XPS/UPS) were performed with a Phoibos 150 instrument equipped with a monochromatic Kα X-ray source (1486.74 eV) at the Institut Catala de Nanociencia i Nanotechnologia (ICN2). The spectra were corrected in energy by using the adventitious carbon peak (C 1s, 284.8 eV) as the reference. Atomic ratios were calculated by integrating elemental peaks with Shirley background profile. For fitting of peaks a combination of Lorentzian and Gaussian functions were utilized. XPS and UPS samples were prepared by treating the films with either TMAI (1 g L^{-1} in methanol for Schlenk-line $AgBiS_2$) or ET (0.2% in methanol for *n*-octylamine $AgBiS_2$). The ligand treatment for Schlenk-line $AgBiS_2$ was carried out as described previously.[17] Fourier transform infrared spectroscopy (FTIR) was performed with a Cary 600 FTIR instrument. For all FTIR measurements, double side polished silicon wafers were used as the substrate. The samples were prepared by spin coating. To evaporate the unbound amines and/or solvents, the samples were annealed on a hot plate at 90 °C. Iodine-amine solution was prepared by dissolving elemental iodine (0.8 mmol) in *n*-octylamine (1 mL) in air. *n*-Octylammonium iodide was prepared by the reaction of *n*-octylamine with hyriodic acid in ethanol. For FTIR measurements, the obtained white powder was spun-coated from ethanol solution.

Device Characterization. Solar cell characterization was performed using a Newport Oriel Sol3A solar simulator equipped with an AM1.5 filter in air. Current−voltage data

https://dx.doi.org/10.1021/acsphotonics.9b01757
ACS Photonics 2020, 7, 588−595

were collected by a Keithley 2400 source meter. For the external quantum efficiency (EQE) measurement, a Stanford Research SR570 transimpedance amplifier connected to a Stanford Research SR830 lock-in amplifier was used. The monochromatic light was generated by a Newport Cornerstone 260 monochromator and the spectrum was corrected using calibrated Newport photodetectors (UV-818 and IR-818) as the reference.

A FiberTech Optica LED lightsource and an Agilent 4000X oscilloscope were used to measure J_{SC} and V_{OC} as a function of light intensity. For J_{SC} and V_{OC}, 50 Ω and 1 MΩ input terminals of the oscilloscope were utilized, respectively. A Vortran Stradus laser with a wavelength of 637 nm was used as the excitation source for transient photovoltage (TPV) and transient photocurrent (TPC) measurements for the calculation of density of states (DOS). See Supporting Information for the details of the calculation.

The thickness of the films was measured using a KLA-Tencor Alpha-Step IQ Surface Profilometer. The films were prepared by spin coating the material on ITO glass, and the measurement point is formed by scratching the film with a sharp metal tip.

■ ASSOCIATED CONTENT

Supporting Information

The Supporting Information is available free of charge at https://pubs.acs.org/doi/10.1021/acsphotonics.9b01757.

The details of DOS and carrier density calculation, Tauc plots and UPS spectra of the nanocrystals, FTIR spectra of the precursors and byproducts of the nanocrystal synthesis, time-dependent performance metrics of the solar cells, SEM images of the $AgBiS_2$ nanocrystal thin films, and the table used for the cost calculation (PDF)

■ AUTHOR INFORMATION

Corresponding Author

Gerasimos Konstantatos − *ICFO-Institut de Ciències Fotòniques, The Barcelona Institute of Science and Technology, 08860 Castelldefels, Barcelona, Spain; ICREA-Institució Catalana de Recerca i Estudis Avançats, 08010 Barcelona, Spain;* orcid.org/0000-0001-7701-8127; Email: gerasimos.konstantatos@icfo.eu

Authors

M. Zafer Akgul − *ICFO-Institut de Ciències Fotòniques, The Barcelona Institute of Science and Technology, 08860 Castelldefels, Barcelona, Spain*

Alberto Figueroba − *ICFO-Institut de Ciències Fotòniques, The Barcelona Institute of Science and Technology, 08860 Castelldefels, Barcelona, Spain*

Santanu Pradhan − *ICFO-Institut de Ciències Fotòniques, The Barcelona Institute of Science and Technology, 08860 Castelldefels, Barcelona, Spain;* orcid.org/0000-0002-8934-4269

Yu Bi − *ICFO-Institut de Ciències Fotòniques, The Barcelona Institute of Science and Technology, 08860 Castelldefels, Barcelona, Spain;* orcid.org/0000-0003-1401-2136

Complete contact information is available at: https://pubs.acs.org/10.1021/acsphotonics.9b01757

Notes

The authors declare no competing financial interest.

■ ACKNOWLEDGMENTS

The authors acknowledge financial support from the European Research Council (ERC) under the European Union's Horizon 2020 research and innovation programme (Grant Agreement No. 725165), the Spanish Ministry of Economy and Competitiveness (MINECO), and the "Fondo Europeo de Desarrollo Regional" (FEDER) through Grant TEC2017-88655-R. The authors also acknowledge financial support from Fundacio Privada Cellex, the program CERCA and from the Spanish Ministry of Economy and Competitiveness, the ICFOstepstone - PhD Programme for Early-Stage Researchers in Photonics, funded by the Marie Skłodowska-Curie Co-funding of regional, national, and international programmes (GA665884) of the European Commission, through the "Severo Ochoa" Programme for Centres of Excellence in R&D (SEV-2015-0522).

■ REFERENCES

(1) Kim, J.; Ouellette, O.; Voznyy, O.; Wei, M.; Choi, J.; Choi, M.-J.; Jo, J. W.; Baek, S.-W.; Fan, J.; Saidaminov, M. I.; et al. Butylamine-Catalyzed Synthesis of Nanocrystal Inks Enables Efficient Infrared CQD Solar Cells. *Adv. Mater.* **2018**, *30* (45), 1803830.

(2) Yang, Z.; Fan, J. Z.; Proppe, A. H.; Arquer, F. P. G. de; Rossouw, D.; Voznyy, O.; Lan, X.; Liu, M.; Walters, G.; Quintero-Bermudez, R.; et al. Mixed-Quantum-Dot Solar Cells. *Nat. Commun.* **2017**, *8* (1), 1325.

(3) Luo, D.; Yang, W.; Wang, Z.; Sadhanala, A.; Hu, Q.; Su, R.; Shivanna, R.; Trindade, G. F.; Watts, J. F.; Xu, Z.; et al. Enhanced Photovoltage for Inverted Planar Heterojunction Perovskite Solar Cells. *Science* **2018**, *360* (6396), 1442−1446.

(4) Tavakoli, M. M.; Tress, W.; Milić, J. V.; Kubicki, D.; Emsley, L.; Grätzel, M. Addition of Adamantylammonium Iodide to Hole Transport Layers Enables Highly Efficient and Electroluminescent Perovskite Solar Cells. *Energy Environ. Sci.* **2018**, *11* (11), 3310−3320.

(5) Bella, F.; Griffini, G.; Correa-Baena, J.-P.; Saracco, G.; Gratzel, M.; Hagfeldt, A.; Turri, S.; Gerbaldi, C. Improving Efficiency and Stability of Perovskite Solar Cells with Photocurable Fluoropolymers. *Science* **2016**, *354* (6309), 203−206.

(6) McDaniel, H.; Fuke, N.; Pietryga, J. M.; Klimov, V. I. Engineered $CuInSe_xS_{2-x}$ Quantum Dots for Sensitized Solar Cells. *J. Phys. Chem. Lett.* **2013**, *4* (3), 355−361.

(7) Aldakov, D.; Lefrançois, A.; Reiss, P. Ternary and Quaternary Metal Chalcogenide Nanocrystals: Synthesis, Properties and Applications. *J. Mater. Chem. C* **2013**, *1* (24), 3756.

(8) Halpert, J. E.; Morgenstern, F. S. F.; Ehrler, B.; Vaynzof, Y.; Credgington, D.; Greenham, N. C. Charge Dynamics in Solution-Processed Nanocrystalline $CuInS_2$ Solar Cells. *ACS Nano* **2015**, *9* (6), 5857−5867.

(9) Li, L.; Coates, N.; Moses, D. Solution-Processed Inorganic Solar Cell Based on in Situ Synthesis and Film Deposition of $CuInS_2$ Nanocrystals. *J. Am. Chem. Soc.* **2010**, *132* (1), 22−23.

(10) Cao, Y.; Denny, M. S.; Caspar, J. V.; Farneth, W. E.; Guo, Q.; Ionkin, A. S.; Johnson, L. K.; Lu, M.; Malajovich, I.; Radu, D.; et al. High-Efficiency Solution-Processed $Cu_2ZnSn(S,Se)_4$ Thin-Film Solar Cells Prepared from Binary and Ternary Nanoparticles. *J. Am. Chem. Soc.* **2012**, *134* (38), 15644−15647.

(11) Du, J.; Du, Z.; Hu, J.-S.; Pan, Z.; Shen, Q.; Sun, J.; Long, D.; Dong, H.; Sun, L.; Zhong, X.; et al. Zn−Cu−In−Se Quantum Dot Solar Cells with a Certified Power Conversion Efficiency of 11.6%. *J. Am. Chem. Soc.* **2016**, *138* (12), 4201−4209.

(12) de Kergommeaux, A.; Fiore, A.; Bruyant, N.; Chandezon, F.; Reiss, P.; Pron, A.; de Bettignies, R.; Faure-Vincent, J. Synthesis of Colloidal $CuInSe_2$ Nanocrystals Films for Photovoltaic Applications. *Sol. Energy Mater. Sol. Cells* **2011**, *95*, S39−S43.

(13) Saha, S. K.; Guchhait, A.; Pal, A. J. Cu_2ZnSnS_4 (CZTS) Nanoparticle Based Nontoxic and Earth-Abundant Hybrid Pn-Junction Solar Cells. *Phys. Chem. Chem. Phys.* **2012**, *14* (22), 8090.

(14) So, D.; Pradhan, S.; Konstantatos, G. Solid-State Colloidal $CuInS_2$ Quantum Dot Solar Cells Enabled by Bulk Heterojunctions. *Nanoscale* **2016**, *8* (37), 16776−16785.
(15) Huang, P.-C.; Yang, W.-C.; Lee, M.-W. $AgBiS_2$ Semiconductor-Sensitized Solar Cells. *J. Phys. Chem. C* **2013**, *117* (36), 18308−18314.
(16) Pai, N.; Lu, J.; Senevirathna, D. C.; Chesman, A. S. R.; Gengenbach, T.; Chatti, M.; Bach, U.; Andrews, P. C.; Spiccia, L.; Cheng, Y.-B.; et al. Spray Deposition of $AgBiS_2$ and Cu_3BiS_3 Thin Films for Photovoltaic Applications. *J. Mater. Chem. C* **2018**, *6* (10), 2483−2494.
(17) Bernechea, M.; Miller, N. C.; Xercavins, G.; So, D.; Stavrinadis, A.; Konstantatos, G. Solution-Processed Solar Cells Based on Environmentally Friendly $AgBiS_2$ Nanocrystals. *Nat. Photonics* **2016**, *10* (8), 521−525.
(18) Jean, J.; Xiao, J.; Nick, R.; Moody, N.; Nasilowski, M.; Bawendi, M.; Bulović, V. Synthesis Cost Dictates the Commercial Viability of Lead Sulfide and Perovskite Quantum Dot Photovoltaics. *Energy Environ. Sci.* **2018**, *11* (9), 2295−2305.
(19) Oh, J. T.; Bae, S. Y.; Ha, S. R.; Cho, H.; Lim, S. J.; Boukhvalov, D. W.; Kim, Y.; Choi, H. Water-Resistant $AgBiS_2$ Colloidal Nanocrystal Solids for Eco-Friendly Thin Film Photovoltaics. *Nanoscale* **2019**, *11* (19), 9633−9640.
(20) Lei, P.; An, R.; Zheng, X.; Zhang, P.; Du, K.; Zhang, M.; Dong, L.; Gao, X.; Feng, J.; Zhang, H. Ultrafast Synthesis of Ultrasmall Polyethylenimine-Protected $AgBiS_2$ Nanodots by "Rookie Method" for *in Vivo* Dual-Modal CT/PA Imaging and Simultaneous Photothermal Therapy. *Nanoscale* **2018**, *10* (35), 16765−16774.
(21) Mak, C. H.; Qian, J.; Rogée, L.; Lai, W. K.; Lau, S. P. Facile Synthesis of $AgBiS_2$ Nanocrystals for High Responsivity Infrared Detectors. *RSC Adv.* **2018**, *8* (68), 39203−39207.
(22) Joo, J.; Na, H. B.; Yu, T.; Yu, J. H.; Kim, Y. W.; Wu, F.; Zhang, J. Z.; Hyeon, T. Generalized and Facile Synthesis of Semiconducting Metal Sulfide Nanocrystals. *J. Am. Chem. Soc.* **2003**, *125* (36), 11100−11105.
(23) Zhong, X.; Liu, S.; Zhang, Z.; Li, L.; Wei, Z.; Knoll, W. Synthesis of High-Quality CdS, ZnS, and $Zn_xCd_{1-x}S$ Nanocrystals Using Metal Salts and Elemental Sulfur. *J. Mater. Chem.* **2004**, *14* (18), 2790−2794.
(24) Roberts, D. M.; Landin, A. R.; Ritter, T. G.; Eaves, J. D.; Stoldt, C. R. Nanocrystalline Iron Monosulfides Near Stoichiometry. *Sci. Rep.* **2018**, *8* (1), 6591.
(25) Baek, I. C.; Seok, S. I.; Pramanik, N. C.; Jana, S.; Lim, M. A.; Ahn, B. Y.; Lee, C. J.; Jeong, Y. J. Ligand-Dependent Particle Size Control of PbSe Quantum Dots. *J. Colloid Interface Sci.* **2007**, *310* (1), 163−166.
(26) Thomson, J. W.; Nagashima, K.; Macdonald, P. M.; Ozin, G. A. From Sulfur-Amine Solutions to Metal Sulfide Nanocrystals: Peering into the Oleylamine-Sulfur Black Box. *J. Am. Chem. Soc.* **2011**, *133*, 5036−5041.
(27) Nagakura, S. Molecular Complexes and Their Spectra. VIII. The Molecular Complex between Iodine and Triethylamine. *J. Am. Chem. Soc.* **1958**, *80* (3), 520−524.
(28) Kirchartz, T.; Deledalle, F.; Tuladhar, P. S.; Durrant, J. R.; Nelson, J. On the Differences between Dark and Light Ideality Factor in Polymer:Fullerene Solar Cells. *J. Phys. Chem. Lett.* **2013**, *4* (14), 2371−2376.
(29) Cowan, S. R.; Roy, A.; Heeger, A. J. Recombination in Polymer-Fullerene Bulk Heterojunction Solar Cells. *Phys. Rev. B: Condens. Matter Mater. Phys.* **2010**, *82* (24), 245207.
(30) Ip, A. H.; Thon, S. M.; Hoogland, S.; Voznyy, O.; Zhitomirsky, D.; Debnath, R.; Levina, L.; Rollny, L. R.; Carey, G. H.; Fischer, A.; et al. Hybrid Passivated Colloidal Quantum Dot Solids. *Nat. Nanotechnol.* **2012**, *7* (9), 577−582.

https://dx.doi.org/10.1021/acsphotonics.9b01757
ACS Photonics 2020, 7, 588−595